

Cite this: *J. Mater. Chem. A*, 2019, 7, 23008

“Twisted” conjugated molecules as donor materials for efficient all-small-molecule organic solar cells processed with tetrahydrofuran†

Xiafei Cheng,^a Miaomiao Li,^{*ab} Ziqi Guo,^d Jinde Yu,^e Guanghao Lu,^{id e} Laju Bu,^e Long Ye,^{id f} Harald Ade,^f Yongsheng Chen,^{id *d} and Yanhou Geng,^{id *abc}

High-performance organic semiconductors that can be processed with environmentally benign solvents are highly desirable for printable optoelectronics. Herein, four acceptor–donor–acceptor conjugated molecules, *i.e.*, DRTT-T, DRTT-R, DRTT-OR and DRTT, with 3-ethylrhodanine as acceptor terminal units and 2,5-bis(4,8-di(5-(2-ethylhexyl)thiophen-2-yl)benzo[1,2-*b*:4,5-*b'*]dithiophen-2-yl)thieno[3,2-*b*]thiophene derivatives as donor units were synthesized. 5-(2-Ethylhexyl)thiophen-2-yl, 2-ethylhexyl and 2-ethylhexyloxy were introduced at the β -positions of the central thieno[3,2-*b*]thiophene (TT) units in DRTT-T, DRTT-R and DRTT-OR, respectively, and unsubstituted TT was used as the central unit in DRTT. As revealed by density functional theory calculations, DRTT-OR and DRTT adopt an almost planar geometry, while DRTT-T and DRTT-R have “twisted” backbones due to the introduction of bulky substituents on TT units. Differing from DRTT-OR and DRTT which are only well soluble in chlorinated solvents such as chloroform, DRTT-T and DRTT-R also show high solubility in “greener” solvents, including toluene and tetrahydrofuran (THF). Non-fullerene small molecule (NFSM) organic solar cells (OSCs) were fabricated with these molecules as donor materials. The molecules (DRTT-T and DRTT-R) with twisted backbones displayed remarkably higher device performance compared to more planar ones (DRTT-OR and DRTT), attributed to the formation of ordered face-on microstructures with π – π stacking distances of 3.7–3.8 Å and interpenetration networks of donor and acceptor components in the blend films based on DRTT-T and DRTT-R. Most importantly, the power conversion efficiencies (PCEs) of DRTT-T and DRTT-R based devices processed with THF reached 9.37% and 10.45%, respectively. This study demonstrates that “twisting” conjugated backbones is an appropriate strategy to design eco-friendly solvent processable organic semiconductors for high-efficiency OSCs.

Received 17th July 2019
Accepted 16th September 2019

DOI: 10.1039/c9ta07760j

rsc.li/materials-a

Introduction

Organic solar cells (OSCs) are considered as a promising solar technology due to their unique advantages of light weight, low

cost, flexibility, and solution based fabrication.^{1–3} Owing to the strong ability to dissolve organic semiconducting materials, chlorinated solvents, such as chloroform (CF), chlorobenzene (CB) and 1,2-dichlorobenzene (*o*-DCB), are the widely-used solvents in OSC fabrication. However, the use of these solvents is restricted in industry since they are highly harmful to human health and the environment. Although some alternative solvents, for example, toluene (Tol) and 1,2,4-trimethylbenzene,^{4–10} could be used to replace highly toxic ones, OSCs often show reduced efficiency mainly because the low solubility of the donor and/or acceptor materials in these solvents results in a poor bulk-heterojunction (BHJ) morphology containing excessively large domains.^{8–10} Thereby, only several BHJ systems (such as PIDTT-DFBT:PC₇₁BM,⁴ PffBT4T-C₉C₁₃:PC₇₁BM⁵ and PBTA-TF:IT-M⁷) processed with non-halogenated solvents are able to obtain high photovoltaic performance comparable to their halogenated solvent processed counterparts. On the other hand, these aromatic solvents still have relatively high toxicity. Therefore, it is of critical importance to develop photoactive materials that are readily soluble in “greener” solvents and

^aSchool of Materials Science and Engineering, Tianjin University, Tianjin 300072, P. R. China. E-mail: miaomiao.li@tju.edu.cn; yanhou.geng@tju.edu.cn

^bTianjin Key Laboratory of Molecular Optoelectronic Science, Collaborative Innovation Center of Chemical Science and Engineering, Tianjin University, Tianjin, P. R. China
^cJoint School of National University of Singapore and Tianjin University, International Campus of Tianjin University, Binhai New City, Fuzhou 350207, P. R. China

^dThe Key Laboratory of Functional Polymer Materials, State Key Laboratory and Institute of Elemento-Organic Chemistry, Centre of Nanoscale Science and Technology, College of Chemistry, Nankai University, Tianjin 300071, China

^eFrontier Institute of Science and Technology, and School of Science, Xi'an Jiaotong University, Xi'an 710049, China

^fDepartment of Physics, Organic and Carbon Electronics Lab (ORaCEL), North Carolina State University, Raleigh NC 27695, USA

† Electronic supplementary information (ESI) available: ¹H NMR and ¹³C NMR spectra, mass spectra, and characterization of TGA, DSC, CV and SCLC. See DOI: 10.1039/c9ta07760j

meanwhile have appropriate aggregation behavior to ensure proper phase separation and ordered molecular packing in BHJ films.

In principle, the solubility of conjugated molecules can be enhanced *via* twisting their conjugated backbones from planarity. However, “over-twisting” is detrimental to the close intermolecular packing, resulting in poor charge transport properties in the film state. The ideal case is that the molecules adopt twisted backbones in solution but planar geometries in the film state. The rotation barrier of twisting the inter-ring C–C linkage could be overcome by intermolecular interactions (such as π – π interaction and hydrogen bonding) in the condensed phase. Therefore, we proposed to modulate steric substituent-induced twisting of the molecules to improve their solubility in eco-friendly solvents, and introduce aromatic units with a large π system as building blocks to facilitate backbone planarization and molecular ordering in the film state.

Compared to polymers, small molecules have well-defined chemical structures and can serve as models for establishing the relationship between the chemical structure and device performance. In addition, conjugated small molecules have shown great potential in the fabrication of OSCs either as donor or acceptor materials due to low batch-to-batch variation.^{11–25} To understand the effects of backbone “twisting” on solubility, film microstructures and photovoltaic performance, in the current paper, we synthesized four small molecule donors, *i.e.*, DRTT-T, DRTT-R, DRTT-OR and DRTT that shared the same conjugated backbones but had different distortion angles between single-bond-linked sub-units, as shown in Fig. 1. DRTT-T and DRTT-R have larger distortion angles and exhibited very good solubility in much “greener” solvent tetrahydrofuran (THF), but could form ordered

microstructures with π – π stacking distances of 3.7–3.8 Å in the film state. In contrast, other two molecules with almost planar geometries are only well soluble in chlorinated solvents such as CF. Non-fullerene all small molecule solar cells (NFSM-OSCs) with DRTT-T or DRTT-R as donor materials were successfully fabricated with THF as the solvent. Power conversion efficiencies (PCEs) of 9.37% and 10.45% have been demonstrated for the devices based on DRTT-T and DRTT-R, respectively. To the best of our knowledge, this is the first report on non-chlorinated solvent processed NFSM-OSCs, and also represents one of the highest efficiencies of OSCs fabricated by using non-aromatic solvents.^{26–30}

Results and discussion

Molecular design principle and density functional theory calculations

Fig. 1a shows the chemical structures of DRTT-T, DRTT-R, DRTT-OR and DRTT. The substituents, *i.e.*, 5-(2-ethylhexyl)thiophen-2-yl, 2-ethylhexyl and 2-ethylhexyloxy with decreased bulkiness, were introduced at the β -positions of the central thieno[3,2-*b*]thiophene (TT) units in DRTT-T, DRTT-R and DRTT-OR, respectively, for adjusting the backbone twisting. Molecular DRTT based on unsubstituted TT was also synthesized for comparison. To encourage the planarization and close intermolecular packing of the molecules in the solid state, 4,8-di(5-(2-ethylhexyl)thiophen-2-yl)benzo[1,2-*b*:4,5-*b'*]dithiophene, a two-dimensional (2D) conjugated unit that has been proved to be able to enhance the π – π interaction of the conjugated polymers,^{31,32} has been selected as another building block. The incorporation of 3-ethylrhodanine electron-withdrawing terminal yields the “acceptor–donor–acceptor” structure to

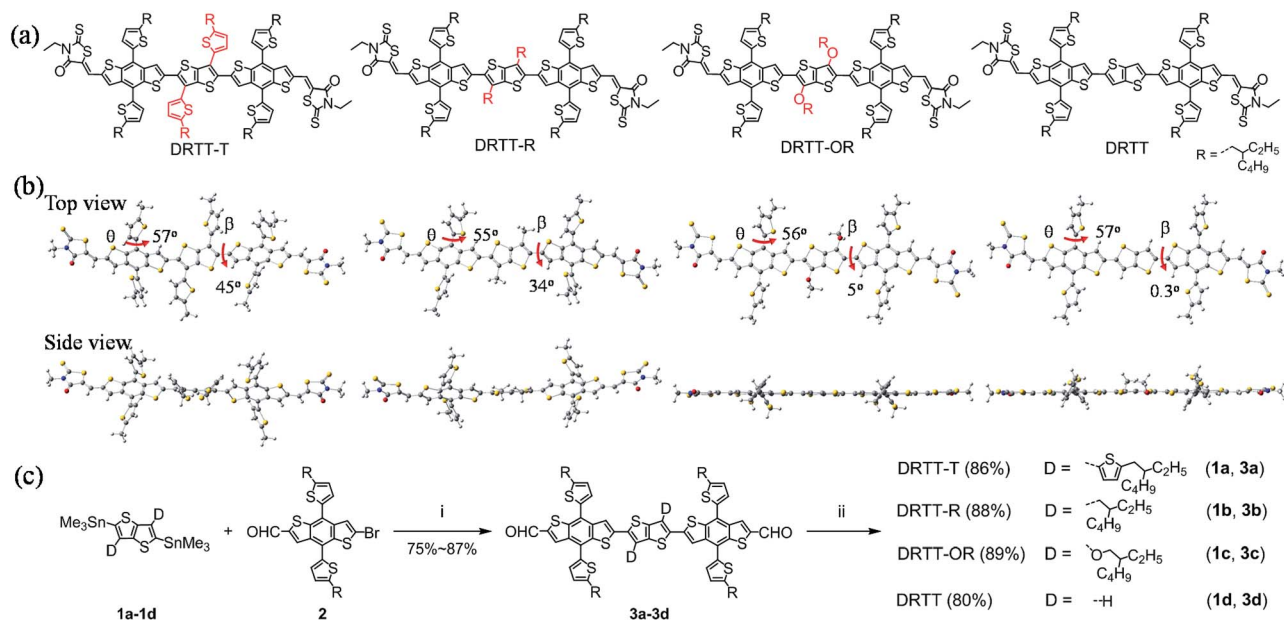


Fig. 1 Chemical structures of DRTT-T, DRTT-R, DRTT-OR and DRTT (a), DFT optimized molecular geometries of the molecules (b) and synthetic route to the molecules (c). Reagents and conditions: (i) Pd(PPh₃)₄, toluene, microwave, 170 °C; (ii) 3-ethyl-2-thioxothiazolidin-4-one, triethylamine, CHCl₃, reflux.

broaden light absorption and further promote intramolecular interactions in the solid state.

Fig. 1b depicts the optimized geometries of DRTT-T, DRTT-R, DRTT-OR and DRTT by using density functional theory (DFT) calculations at the B3LYP/6-31g(d) level. All alkyl substituents were replaced with methyl groups for simplifying the calculations. For all molecules, the benzo[1,2-*b*:4,5-*b'*] dithiophene (BDT) spacer and its adjacent terminal unit are coplanar, and there are similar torsion angles (55–57°) between BDT and its alkylthiophene side chains. The major difference lies in the torsion angles between the TT unit and its adjacent BDT spacers for the four molecules. DRTT-OR and DRTT are almost planar as revealed by very small torsion angles of 5° and 0.3° between BDT and TT units, respectively. In contrast, DRTT-T and DRTT-R are significantly twisted with the torsion angles between BDT and TT units of 45° for DRTT-T and 34° for DRTT-R. Previous reports showed that the introduction of alkoxy groups could improve the planarity of conjugated molecules due to the occurrence of the weak S...O intramolecular interaction.^{33–35} Here, no such type of interaction was observed and 2-ethylhexyloxy acted as a substituent with small steric hindrance. These molecules were more twisted with the increase of the bulkiness of the substituents (H < 2-ethylhexyloxy < 2-ethylhexyl < 5-(2-ethylhexyl)thiophen-2-yl), as we expected.

Materials synthesis, thermal stability and solubility

The synthetic route to DRTT-T, DRTT-R, DRTT-OR and DRTT is shown in Fig. 1c. Microwave-assisted Stille coupling of compounds **1a–d** and **2** afforded compounds **3a–d** in yields of 75–87%. Subsequent Knoevenagel condensations gave DRTT-T, DRTT-R, DRTT-OR and DRTT in good yields. The synthetic details are outlined in the ESI.† The chemical structures of DRTT-T, DRTT-R, DRTT-OR and DRTT were verified by NMR spectra (Fig. S1–S16†), matrix-assisted laser desorption ionization time-of-flight (MALDI-TOF) mass spectra (Fig. S17–S24†) and elemental analyses. Thermogravimetric analyses (TGA) revealed that DRTT-T, DRTT-R, DRTT-OR and DRTT have good thermal stability with 5% weight loss temperatures (T_d) at 364, 387, 381 and 416 °C, respectively (Fig. S25†).

The solubility of the four molecules was tested. DRTT-T and DRTT-R are highly soluble in common chlorinated solvents (such as CF, CB and *o*-DCB), with a solubility of 95 and 92 mg

mL⁻¹ in CF at room temperature, which are much higher than those of DRTT-OR (29 mg mL⁻¹) and DRTT (8 mg mL⁻¹). In addition to the planar backbones, the low solubility of DRTT is also caused by the fewer alkyl side chains. Besides, DRTT-T and DRTT-R with twisted structures can also be easily dissolved in some non-halogenated solvents, such as Tol and THF, and their solubilities in THF are 45 and 41 mg mL⁻¹ at room temperature, respectively. By contrast, DRTT-OR and DRTT show a much poorer solubility of 7 and 5 mg mL⁻¹, respectively, in THF. The superior solubility of DRTT-T and DRTT-R could be ascribed to their twisted backbones, as aforementioned.

Photophysical and electrochemical properties

The solution and film absorption spectra of the molecules are illustrated in Fig. 2. In solution, all four molecules showed featureless absorption spectra with absorption maxima (λ_{max}) at 532, 534, 583 and 555 nm for DRTT-T, DRTT-R, DRTT-OR and DRTT, respectively. A >20 nm blue shift and much lower absorption coefficient were observed for the spectra of DRTT-T and DRTT-R compared to that of DRTT. This is consistent with the twisted backbones of DRTT-T and DRTT-R. In contrast, DRTT-OR showed a remarkably red-shifted spectrum due to its almost planar structure and the strong electron-donating characteristics of the alkoxy group. From solution to films, all molecules displayed red-shifted and broadened absorption spectra, caused by intermolecular interactions in the solid state. Compared to the as-cast films of DRTT-OR and DRTT that exhibited obvious vibronic peaks, DRTT-T and DRTT-R as-cast films showed much weaker absorption shoulders. Especially, the spectrum of DRTT-T was almost featureless. This phenomenon indicates that the molecules of DRTT-T and DRTT-R might pack more disorderedly. After solvent vapor annealing (SVA), the absorption shoulder peaks of DRTT-R and DRTT-OR films were enhanced (Fig. 2c), suggesting improved molecular packing. The film absorption spectrum featuring well-defined vibronic peaks was also observed for DRTT-T, implying the formation of ordered microstructures in which molecules adopted a planar geometry.^{36–38} In contrast, the absorption spectrum of DRTT was almost unchanged after SVA. This means that the final state was already achieved before SVA. The optical bandgaps (E_g^{opt}) of these molecules calculated from the absorption onset of the SVA-treated films were 1.83–1.86 eV

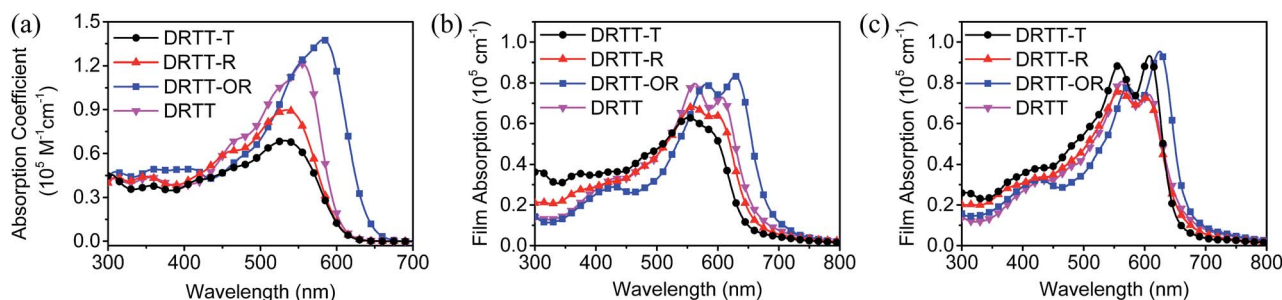


Fig. 2 Absorption spectra of DRTT-T, DRTT-R, DRTT-OR and DRTT in chloroform solutions (a, 10^{-5} mol L⁻¹ in chloroform) and in thin films without post-treatment (b) and with SVA using CF for 80 s (c).

for DRTT-T, DRTT-R and DRTT, while DRTT-OR exhibited a smaller E_g^{opt} of 1.79 eV. Electrochemical cyclic voltammetry (CV, see Fig. S26†) was employed to estimate the highest occupied molecular orbital (HOMO) and the lowest unoccupied molecular orbital (LUMO) energy levels of the molecules. As shown in Table 1, the HOMO and LUMO energy levels were -5.39 and -3.35 eV for DRTT-T, -5.40 and -3.24 eV for DRTT-R, -5.31 and -3.36 eV for DRTT-OR, and -5.29 and -3.23 eV for DRTT, respectively. The lower bandgap of DRTT-OR could be ascribed to its relatively low-lying LUMO and high-lying HOMO energy levels.

Packing behavior of the molecules

Packing structures of the molecules in thin films were investigated by X-ray diffraction (XRD). Here CF was used to make the films as it is a good solvent for all four molecules. The out-of-plane and in-plane XRD patterns are shown in Fig. 3, and the d -spacings and the crystalline coherence lengths of the molecules are summarized in Tables S1 and S2.† The as-cast films of DRTT-R, DRTT-OR and DRTT all showed pronounced (100) diffraction peaks in the out-of-plane patterns. The (200) and even (300) peaks in the out-of-plane direction as well as obvious (010) diffraction peaks in the in-plane direction were also observed for DRTT-OR and DRTT. In contrast, only a weak and broad (100) diffraction peak was observed for DRTT-T. These observations indicate that DRTT-OR and DRTT already formed 2D ordered edge-on nanostructures in the as-cast films, while DRTT-R only formed one-dimensional ordered lamellar nanostructures and DRTT-T packed in an almost disordered way. SVA was used to improve the intermolecular packing, and CF was chosen as the annealing solvent since it is a good solvent for all four molecules. SVA had a negligible influence on the XRD patterns of the DRTT film, while both in-plane and out-of-plane diffraction peaks of DRTT-OR became sharper and stronger, suggesting the formation of more ordered 2D nanostructures. In addition to the enhanced (100) peak, the (010) diffraction peak also appeared for DRTT-R. SVA caused a huge change of the XRD pattern of DRTT-T, which carries the largest substituents in the TT unit. Sharp and strong (100) diffraction as well as obvious (200) and (010) diffractions in the out-of-plane XRD pattern were observed, indicative of the formation of ordered films. All the above phenomena are consistent with the results of the absorption spectra measurements and our expectation in

molecular design. The molecules (DRTT and DRTT-OR) with relatively planar structures self-organized very fast in the film forming process. The introduction of bulky substituents on the TT unit improves the solubility of the molecules but retards the formation of ordered films due to the steric hindrance caused by the substituents. However, ordered nanostructures in which the molecules adopt a planar geometry could be formed facilitated by the strong intermolecular π - π interaction, once the self-organization time is long enough (SVA gave enough time for the self-organization of the molecules).

The lamellar packing d -spacings of the molecules derived from the out-of-plane (100) diffraction peaks followed the order of DRTT (16.06 Å) < DRTT-R (18.21 Å) < DRTT-OR (18.78 Å) < DRTT-T (19.41 Å), which could be related to the length of the side chains on the TT unit. The (010) peaks are located at 23.8° for DRTT-T, 23.3° for DRTT-R, 23.6° for DRTT-OR and 24.4° for DRTT, corresponding to the π - π stacking distances of 3.74, 3.79, 3.77 and 3.66 Å, respectively. Clearly, DRTT-T and DRTT-R formed relatively close intermolecular stacking with similar (010) d -spacings to that of DRTT-OR. The small π - π stacking distance of DRTT could be ascribed to no side chains on its TT unit. It is interesting to note that DRTT exhibited the weakest (010) diffraction among the four molecules. This means that the introduction of the substituents on the TT unit promotes the π - π interaction. Previous reports have shown that using alkylthiophene as side chains of conjugated polymers could promote the π - π stacking of the conjugated backbones.^{31,39–41} Note that the out-of-plane (010) diffraction peaks were much stronger than the (010) diffraction peaks in the in-plane patterns of DRTT-T and DRTT-R, indicative of the preferential face-on orientation of the backbones, which is desirable for the OSC geometry. Different from DRTT-T and DRTT-R, DRTT-OR and DRTT in films presented solely edge-on orientation, as revealed by the pronounced (010) peak in the in-plane direction and intense ($h00$) diffraction peaks in the out-of-plane direction.

Photovoltaic properties

The solubility of DRTT-OR and DRTT in THF was rather low. Then the devices with THF as the solvent were only fabricated using DRTT-T and DRTT-R as donor materials. A device architecture of indium tin oxide (ITO)/poly(3,4-ethylenedioxythiophene):polystyrenesulphonate (PEDOT:PSS)/active layer/PDINO⁴² (Fig. S27†)/Al was employed (Fig. 4a). F-

Table 1 Photophysical and electrochemical parameters of the molecules

| Molecule | λ_{max} (nm) | | | E_g^{optc} (eV) | LUMO ^d (eV) | HOMO ^d (eV) |
|----------|-----------------------------|-------------------|-------------------|--------------------------|------------------------|------------------------|
| | Solution | Film ^a | Film ^b | | | |
| DRTT-T | 532 | 555 | 556, 608 | 1.86 | -3.35 | -5.39 |
| DRTT-R | 534 | 560, 597 | 557, 604 | 1.83 | -3.24 | -5.40 |
| DRTT-OR | 583 | 581, 628 | 571, 624 | 1.79 | -3.36 | -5.31 |
| DRTT | 555 | 562, 606 | 562, 606 | 1.83 | -3.23 | -5.29 |

^a Films without post-treatment. ^b Films with SVA using CF for 80 s. ^c The optical bandgap E_g^{optc} was calculated from the absorption onset of the SVA-treated film. ^d The HOMO and LUMO energy levels were calculated according to $E_{\text{HOMO}} = -(4.80 + E_{\text{onset}}^{\text{ox}})$ eV and $E_{\text{LUMO}} = -(4.80 + E_{\text{onset}}^{\text{re}})$ eV, in which $E_{\text{onset}}^{\text{ox}}$ and $E_{\text{onset}}^{\text{re}}$ represent oxidation and reduction onset potentials, respectively, versus the half potential of Fc/Fc⁺.

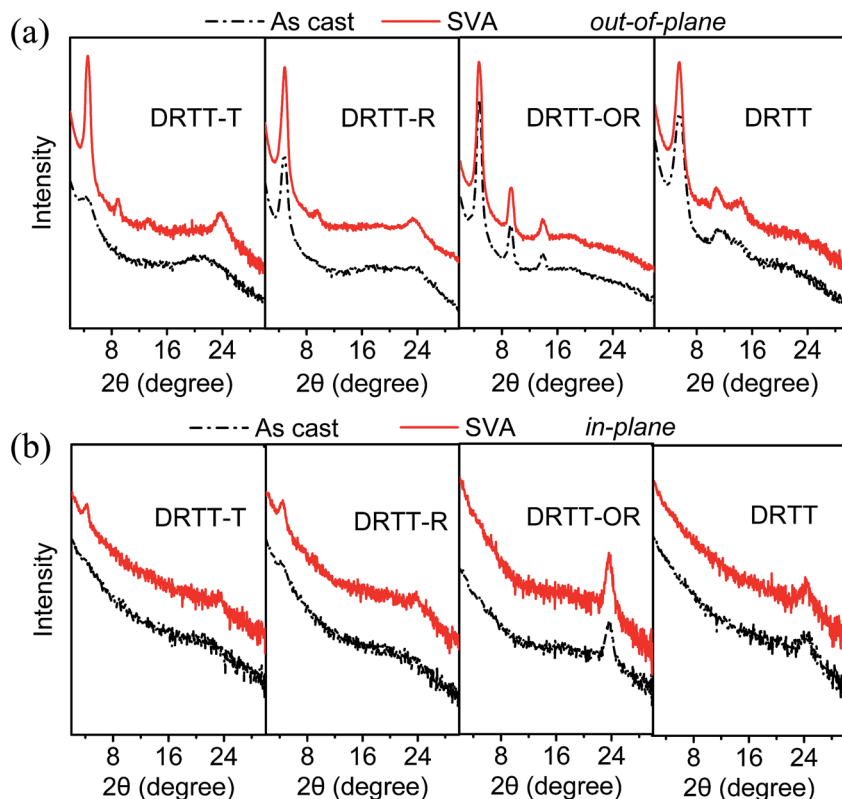


Fig. 3 Out-of-plane (a) and in-plane (b) XRD patterns of DRTT-T, DRTT-R, DRTT-OR and DRTT neat films without post-treatment and with SVA using CF for 80 s.

2Cl^{43} (Fig. 4b) was used as the acceptor material since it has appropriate HOMO/LUMO levels ($-5.68/-3.89$ eV) and is highly soluble in THF (40 mg mL^{-1}). The detailed device data obtained

from different fabrication conditions, including donor/acceptor weight ratios, active layer thicknesses and post treatments, are outlined in Tables S3–S7.† The optimized devices were

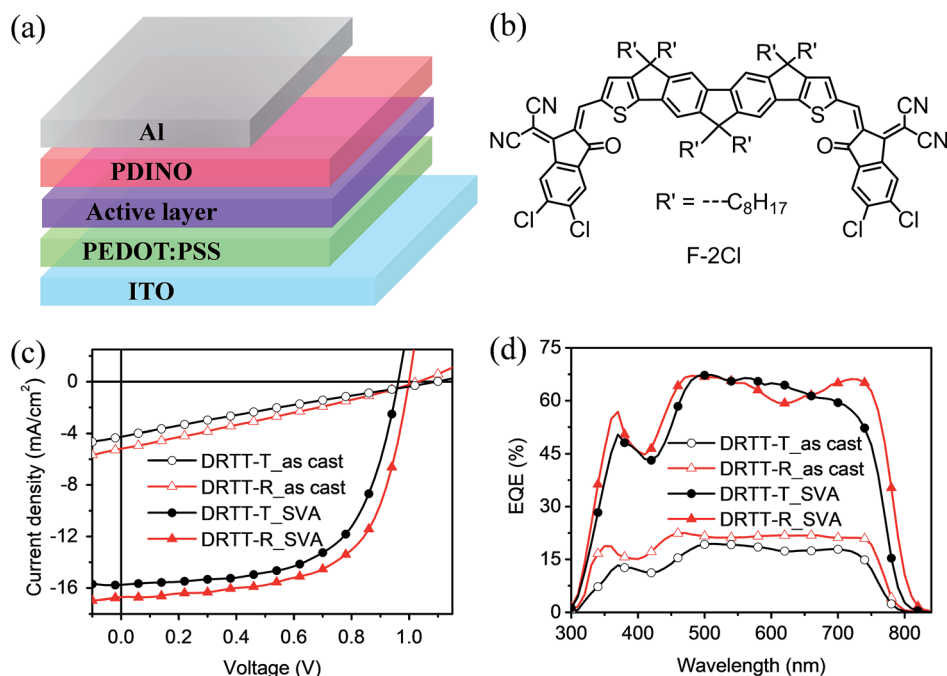


Fig. 4 Device architecture of the NFSM-OSCs (a), chemical structure of F-2Cl (b), and current density–voltage (J – V) characteristics (c) and the external quantum efficiency (EQE) curves (d) of THF-processed OSCs based on DRTT-T and DRTT-R without and with SVA treatments.

fabricated with a donor/acceptor weight ratio of 1 : 0.75 and an active-layer thickness of ~ 120 nm. The typical current density–voltage (J – V) curves of the devices are shown in Fig. 4c, and the corresponding photovoltaic parameters are summarized in Table 2. Without post-treatment, the devices based on DRIT-T and DRIT-R showed low PCEs of 1.10% and 1.46%, respectively, with short-circuit current densities (J_{sc} s) of 4–5 mA cm⁻² and fill factors (FFs) < 30%. The poor intermolecular π – π stacking could be a main reason for the low FFs and J_{sc} s of the devices. According to the above XRD studies on the neat films of donor materials, SVA can promote the mobility of the donor molecules and then improve the packing order of the molecules. Thus, SVA was employed to further optimize the device performance. Since the vapor pressure of the annealing solvent would influence crystallization and aggregation of donor and acceptor molecules,⁴⁴ CF and Tol that have different boiling points were chosen as the annealing solvents. The details for the SVA of the blend films are illustrated in the ESI. For the control of the crystallization and the length scale of phase separation, the SVA conditions were systematically screened by varying the volume of the annealing solvent and the SVA time (see Tables S3–S7†). As shown in Table 2, after SVA, the devices delivered a large improvement in J_{sc} s and FFs, and thus dramatically enhanced PCEs. The small drop in open-circuit voltages (V_{oc} s) could originate from the change of quasi-Fermi levels of the donor and acceptor after SVA treatment,^{45,46} and this phenomenon was also observed in the literature.^{13,44,47–50} The device based on DRIT-T presented a PCE of 9.37% with a V_{oc} of 0.95 V, a J_{sc} of 15.72 mA cm⁻² and a FF of 62.8% after CF vapour annealing, and a lower PCE of 8.06% was obtained for the Tol-treated devices. For DRIT-R based devices, the best photovoltaic performance was achieved upon SVA with Tol. A maximum PCE of 10.45% was obtained with a V_{oc} of 1.00 V, a J_{sc} of 16.82 mA cm⁻² and a FF of 62.6%. Fig. 4d shows the external quantum efficiency (EQE) curves of the devices under different conditions. The devices with SVA gave much higher EQE than those of the untreated devices over the entire photo-to-current response range. The maximum EQE values of SVA-treated

DRIT-T and DRIT-R based devices reached 67.1% and 67.3%, respectively. Compared to the DRIT-T based device, the DRIT-R based device exhibited a broader EQE response with a red-shifted edge at ~ 820 nm, which was in good agreement with the absorption spectra of the blend films (Fig. S28†). The calculated J_{sc} s estimated from the integration of the EQE curves coincide with those extracted from the J – V measurements within an acceptable deviation below 5%.

The stability of the devices based on DRIT-T:F-2Cl and DRIT-R:F-2Cl was preliminarily tested under three different conditions. For comparison, the stabilities of the devices based on widely used polymer donors PBDB-T (for the chemical structure see Fig. S29†) and F-2Cl were also investigated. First, the device storage stability was studied under dark conditions in an argon-filled glove box at room temperature. In this aging measurement, all the devices showed relatively good stability. After 288 h storage, the devices based on DRIT-T, DRIT-R and PBDB-T retained $\sim 92\%$, 86% and 87% of their initial PCEs, respectively (Fig. S30†). The device stability was also investigated under continuous illumination (AM 1.5G, 100 mW cm⁻²) and heating at 60 °C in an argon atmosphere (Fig. S31 and S32†). After 65 h illumination, the PCEs of the devices dropped to ca. 54%, 52% and 58% of the initial values for DRIT-T, DRIT-R and PBDB-T, respectively. After 65 h heating, the PCEs of the devices fell to about 65%, 58% and 70% of the initial values for DRIT-T, DRIT-R and PBDB-T, respectively. Compared to PBDB-T based devices, DRIT-T and DRIT-R based devices exhibited comparable stability under the dark conditions, and slightly lower photo and thermal stability. This implies that the stability of the OSCs based on small molecules can be improved to the comparable level of OSCs based on polymer donors through rational molecular design. From atomic force microscopy (AFM) images (Fig. S33†), no obvious morphology change was observed for the blend films of DRIT-T:F-2Cl, DRIT-R:F-2Cl and PBDB-T:F-2Cl after continuous light illumination and thermal annealing. The rapid degradation in the device performance under photo and thermal stress could be related to the conventional device architecture.⁵¹

Table 2 Photovoltaic performance of the OSCs based on the molecules under different conditions

| Solvent | Donor | Treatment | V_{oc}^a (V) | J_{sc}^a (mA cm ⁻²) | J_{sc}^b (mA cm ⁻²) | FF ^a (%) | PCE ^a (%) |
|---------|---------|------------------|--------------------|-----------------------------------|-----------------------------------|---------------------|----------------------|
| THF | DRIT-T | As cast | 1.10 (1.09 ± 0.01) | 4.26 (4.01 ± 0.20) | 4.17 | 23.5 (21.9 ± 1.0) | 1.10 (0.88 ± 0.17) |
| | | SVA ^c | 0.95 (0.94 ± 0.01) | 15.72 (15.52 ± 0.16) | 15.05 | 62.8 (61.2 ± 1.2) | 9.37 (9.12 ± 0.20) |
| | DRIT-R | As cast | 1.03 (1.02 ± 0.01) | 5.19 (4.98 ± 0.18) | 5.21 | 27.3 (25.8 ± 1.1) | 1.46 (1.25 ± 0.18) |
| | | SVA ^d | 1.00 (0.99 ± 0.01) | 16.82 (16.59 ± 0.17) | 16.11 | 62.6 (61.1 ± 0.9) | 10.45 (10.19 ± 0.21) |
| CF | DRIT-T | As cast | 1.10 (1.09 ± 0.01) | 7.73 (7.49 ± 0.19) | 7.69 | 29.3 (27.6 ± 1.2) | 2.49 (2.21 ± 0.23) |
| | | SVA ^c | 0.95 (0.94 ± 0.01) | 14.96 (14.71 ± 0.21) | 14.99 | 65.7 (64.1 ± 1.1) | 9.32 (9.06 ± 0.22) |
| | DRIT-R | As cast | 1.08 (1.07 ± 0.01) | 6.87 (6.60 ± 0.23) | 6.92 | 27.8 (26.0 ± 1.2) | 2.06 (1.81 ± 0.20) |
| | | SVA ^d | 1.00 (0.99 ± 0.01) | 16.99 (16.75 ± 0.20) | 16.26 | 59.9 (58.5 ± 0.9) | 10.13 (9.87 ± 0.21) |
| | DRIT-OR | As cast | 0.92 (0.91 ± 0.01) | 9.48 (9.26 ± 0.17) | 9.07 | 45.4 (44.0 ± 0.8) | 3.96 (3.72 ± 0.18) |
| | | SVA ^d | 0.88 (0.87 ± 0.01) | 14.23 (14.00 ± 0.18) | 14.61 | 55.6 (54.1 ± 0.9) | 6.95 (6.71 ± 0.19) |
| | DRIT | As cast | 0.99 (0.98 ± 0.01) | 9.36 (9.07 ± 0.25) | 10.24 | 52.3 (50.8 ± 0.9) | 4.85 (4.55 ± 0.25) |
| | | SVA ^d | 0.97 (0.96 ± 0.01) | 8.15 (7.89 ± 0.26) | 9.80 | 50.4 (48.6 ± 1.2) | 4.00 (3.71 ± 0.23) |

^a Optimal and statistical results are listed outside of parentheses and in parentheses, respectively. The average values are obtained from over 20 devices. ^b The calculated J_{sc} s estimated from the integration of the EQE curves. ^c The SVA treatment was conducted with CF for 80 s. ^d The SVA treatment was conducted with Tol for 65 s.

To evaluate the difference in the photovoltaic performance between the molecules with twisted and planar structures, the OSCs were also fabricated with CF as the solvent. The detailed device data are listed in Tables 2 and S8,[†] and typical J - V curves and EQE spectra of the devices are shown in Fig. S34.[†] Similar PCEs were achieved for DRTT-R and DRTT-T based devices, which were 10.13% and 9.32%, respectively. Nevertheless, inferior photovoltaic performance was observed for DRTT and DRTT-OR based devices. The device based on DRTT-OR delivered an optimized PCE of 6.95% under SVA treatment. For DRTT, the device based on the as-cast film gave better photovoltaic performance (PCE = 4.85%) than that of the device based on the SVA-treated film (PCE = 4.00%).

Charge transport and recombination

The hole and electron mobilities (μ_h and μ_e) of DRTT-T and DRTT-R based blend films processed with THF and the blend films based on the four molecules processed with CF were measured using the space-charge-limited-current (SCLC) method, and the results are shown in Table S9 and Fig. S35 and S36.[†] After SVA treatment, DRTT-T:F-2Cl and DRTT-R:F-2Cl films with THF or CF as the solvent and the CF-processed DRTT-OR:F-2Cl film all showed increased μ_h and μ_e , while the DRTT:F-2Cl film showed slightly decreased charge mobility. Under the optimized conditions, DRTT-T:F-2Cl and DRTT-R:F-2Cl exhibited higher μ_h (2.1 – $2.8 \times 10^{-4} \text{ cm}^2 \text{ V}^{-1} \text{ s}^{-1}$) and μ_e ($\sim 1.4 \times 10^{-4} \text{ cm}^2 \text{ V}^{-1} \text{ s}^{-1}$) regardless of CF or THF as the processing solvent, in comparison to those of DRTT-OR:F-2Cl ($\mu_h = 1.37 \times 10^{-4} \text{ cm}^2 \text{ V}^{-1} \text{ s}^{-1}$, $\mu_e = 1.15 \times 10^{-4} \text{ cm}^2 \text{ V}^{-1} \text{ s}^{-1}$) and DRTT:F-2Cl ($\mu_h = 1.13 \times 10^{-4} \text{ cm}^2 \text{ V}^{-1} \text{ s}^{-1}$, $\mu_e = 0.89 \times 10^{-4} \text{ cm}^2 \text{ V}^{-1} \text{ s}^{-1}$) blend films. The high charge mobility of DRTT-T:F-2Cl and DRTT-R:F-2Cl blend films is the key factor for the high J_{sc} s and FFs in the OSCs.

The charge generation and recombination dynamics of the OSC devices were investigated to further probe the reason of the high photovoltaic performance of the molecules with twisted structures. The photocurrent density (J_{ph}) versus effective voltage (V_{eff}) for the devices based on DRTT-T and DRTT-R with THF as the solvent and the devices based on the four molecules with CF as the solvent was measured (Fig. 5a and b). The J_{ph} reached a saturation value (saturation current density, J_{sat}) at high V_{eff} for these devices. Under the short-circuit conditions, the ratios of J_{ph}/J_{sat} were 95.2% and 94.5% for DRTT-T and DRTT-R based THF-devices, and 94.4% and 93.4% for DRTT-T and DRTT-R based CF-devices, respectively. Under the maximal power output conditions, the ratios of DRTT-T and DRTT-R based THF-devices were 78.8% and 75.8%, and the ratios of DRTT-T and DRTT-R based CF-devices were 79.1% and 73.2%, respectively. DRTT-OR and DRTT based CF-devices showed lower J_{ph}/J_{sat} ratios of 91.6% and 88.9% under the short-circuit conditions, and 69.9% and 60.7% under the maximal power output conditions, respectively, indicative of less efficient exciton dissociation and charge collection. Besides, compared to the THF-devices based on DRTT-T ($J_{sat} = 16.51 \text{ mA cm}^{-2}$) and DRTT-R ($J_{sat} = 17.80 \text{ mA cm}^{-2}$) and the CF-devices based on DRTT-T ($J_{sat} = 15.71 \text{ mA cm}^{-2}$), DRTT-R ($J_{sat} = 18.20 \text{ mA cm}^{-2}$) and DRTT-OR ($J_{sat} = 15.53 \text{ mA cm}^{-2}$), the DRTT based CF-device showed a much lower J_{sat} of 9.16 mA cm^{-2} , implying a low exciton generation rate. Fig. 5c–f show transient photocurrent and photovoltage decay kinetics of the devices.^{52,53} The charge sweep-out time under short-circuit conditions was 0.60 and 0.40 μs for DRTT-T and DRTT-R based THF-devices, and 0.60 and 0.31 μs for DRTT-T and DRTT-R based CF-devices, respectively. DRTT-OR and DRTT based CF-devices exhibited a longer charge sweep-out time of 0.75 and 0.78 μs , respectively, which could be related to the lower charge

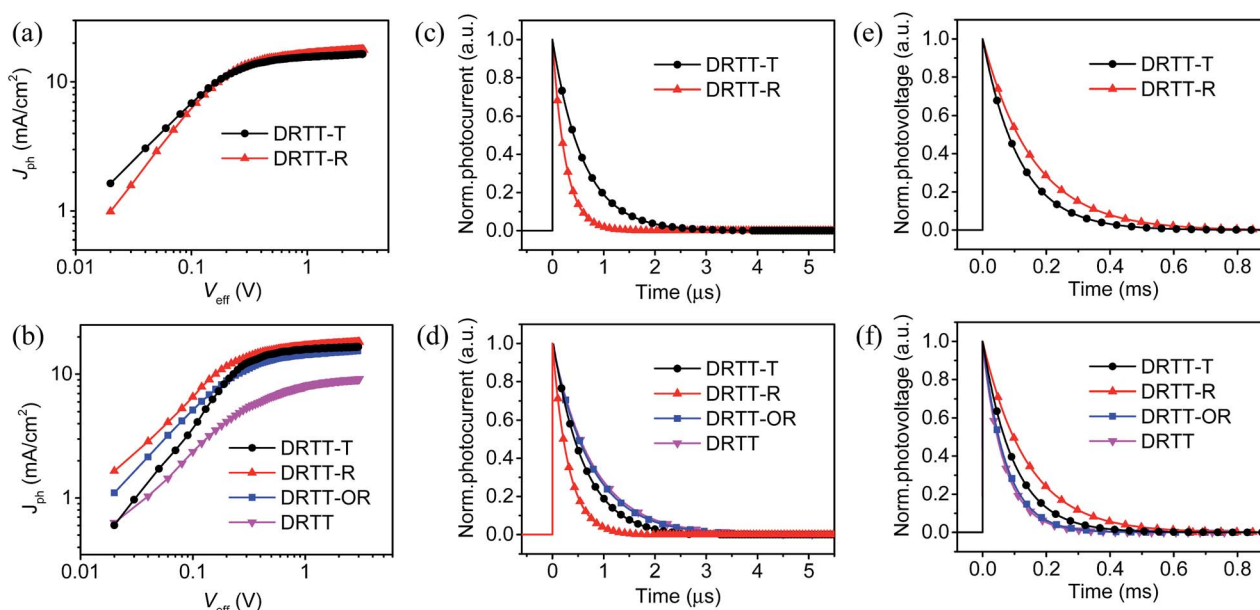


Fig. 5 The photocurrent density versus effective voltage (J_{ph} - V_{eff}) characteristics (a and b), and transient photocurrent (c and d) and transient photovoltage (e and f) measurements of the SVA-treated OSCs with THF (a, c, and e) or CF (b, d, and f) as the processing solvent.

mobility. The carrier lifetimes calculated from the traces of transient photovoltage measurements were 68 and 72 μs for DRTT and DRTT-OR based CF-devices, respectively, while DRTT-T and DRTT-R based devices with THF/CF as the solvent exhibited longer carrier lifetimes of 97/115 and 105/110 μs , respectively. Since the lifetime of carriers at open-circuit voltage is dominated by recombination, the much longer carrier lifetime in DRTT-T and DRTT-R based devices may indicate less charge recombination, which is consistent with the superior J_{sc} and FF values.

Film microstructures and surface morphology

In order to fully understand the high-performance of the THF-processed OSCs based on DRTT-T:F-2Cl and DRTT-R:F-2Cl, the molecular packing in the neat films and the blend films was studied by 2D-GIWAXS (Fig. 6a and S37–S39[†]).⁵⁴ After SVA, more ordered molecular packing was observed for the neat donor (with CF as the annealing solvent for DRTT-T and Tol as the annealing solvent for DRTT-R) (Fig. S37[†]) and acceptor films (with CF or Tol as the annealing solvent) (Fig. S38[†]), and all neat films (DRTT-T, DRTT-R and F-2Cl) exhibit more preferential face-on molecular orientation. The blend films with SVA also showed improved crystallinity in both in-plane and out-of-plane directions compared to their as-cast blend films, as revealed by the stronger diffraction peaks. According to the 2D-GIWAXS patterns of the neat donor and acceptor films, the low- q diffraction peaks along out-of-plane and in-plane directions in the SVA-treated blend films could be ascribed to the (100) diffraction of the small molecule donors, and the overlapped lamellar packing of the donors and the acceptor, respectively. The (100) diffraction peaks in the out-of-plane direction are located at 0.31 and 0.34 \AA^{-1} for DRTT-T:F-2Cl and DRTT-R:F-2Cl, corresponding to the donor lamellar d -spacings of 19.98 and 18.27 \AA , respectively. DRTT-T:F-2Cl and DRTT-R:F-2Cl

blend films displayed pronounced (010) diffraction peaks at 1.66 and $\sim 1.64 \text{\AA}^{-1}$ in the out-of-plane direction arising from the π - π stacking of the donors, giving d -spacings of 3.78 and $\sim 3.83 \text{\AA}$, respectively. The (010) peaks existed at $\sim 1.81 \text{\AA}^{-1}$ in the out-of-plane direction coming from F-2Cl in both SVA-treated blend films with a π - π stacking distance of $\sim 3.47 \text{\AA}$. These results imply that both of the donors and the acceptor showed preferential face-on molecular stacking in the blend films, which is a benefit for the charge transport in OSC devices with vertical sandwich architecture. Moreover, the π - π stacking of the acceptor molecules in the DRTT-R:F-2Cl film was more ordered than those in the DRTT-T:F-2Cl film, which may be a reason for the superior photovoltaic performance of DRTT-R based devices.

The molecular packing in the CF-processed neat and blend films treated with the same annealing solvent (CF for DRTT-T, Tol for DRTT-R, DRTT-OR and DRTT) as the optimized OSC devices was also studied by XRD (Fig. S40 and S41[†]). As discussed above (Fig. 3), DRTT-T presented preferred face-on molecular packing in the CF-annealed neat film. Different from the case with CF as the annealing solvent, DRTT-R showed both face-on and edge-on alignments in the Tol-annealed neat film as indicated by the obvious (010) diffraction peaks in both in-plane and out-of-plane XRD patterns. Tol-annealed DRTT-OR and DRTT neat films still displayed preferential edge-on molecular packing, similar to their CF-annealed counterparts (Fig. 3). In all neat and blend films, F-2Cl retained the face-on molecular stacking. The donor molecules in DRTT-T:F-2Cl and DRTT-R:F-2Cl blend films exhibited preferential face-on orientation, and DRTT-OR showed both face-on and edge-on molecular orientations in the blend film. For the DRTT:F-2Cl blend film, the donor molecules displayed solely edge-on orientation. The incompatible stacking orientations of donor and acceptor molecules could be unfavorable for charge separation.

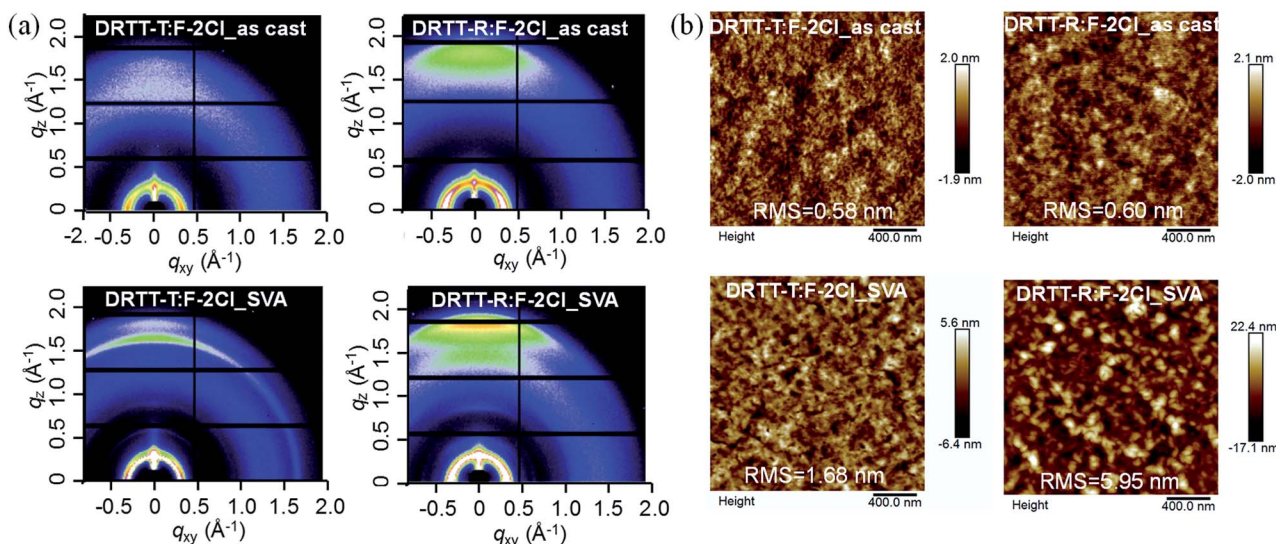


Fig. 6 2D-GIWAXS patterns (a) and AFM images (b) of DRTT-T:F-2Cl and DRTT-R:F-2Cl blend films processed with THF under different conditions.

The morphology of DRTT-T:F-2Cl and DRTT-R:F-2Cl blend films processed with THF was investigated by AFM. As shown in the AFM images (Fig. 6b), DRTT-T:F-2Cl and DRTT-R:F-2Cl blend films without post-treatment presented uniform and smooth features with a root-mean-square (RMS) roughness of 0.58 and 0.60 nm, respectively, and the RMS values increased to 1.68 and 5.95 nm, respectively, after SVA treatment. The SVA-treated blend films showed more pronounced phase separation and better interpenetrating networks of donor and acceptor phases, which could favor charge transport and surpass charge recombination. For comparison, the morphology of the CF-processed blend films based on the four molecule donors was also studied (Fig. S42[†]). DRTT-R:F-2Cl and DRTT-T:F-2Cl blend films processed with CF showed similar morphological features to their counterparts with THF as the solvent. In the as-cast DRTT-OR:F-2Cl film, there were small aggregates which could obstruct charge transport, and more continuous networks with domain sizes of ~ 110 nm were observed in the SVA-treated film. The DRTT:F-2Cl film without post-treatment displayed large domains with a size of 80–100 nm, and the domains became larger upon SVA treatment thus resulting in the decreased photovoltaic performance. Clearly, both of the optimized DRTT:F-2Cl (without post-treatment) and DRTT-OR:F-2Cl (with SVA) films presented excessive phase separation, which could be derived from the strong aggregation ability of DRTT and DRTT-OR. The poor film morphology could induce less efficient exciton dissociation with unfavorable exciton recombination.

The vertical composition distribution of the donor and acceptor components in the blend films also has a large impact on the charge transport and collection processes and hence the photovoltaic performance. Thus, film-depth-dependent light absorption spectra (FLAS) of the blend films without and with SVA treatments on ITO/PEDOT:PSS substrates were recorded (Fig. S43[†] and 7). The experimental and numerical simulation methods have been demonstrated in the literature.^{55–58} As

shown in Fig. 7, the absorption at around 750 nm is contributed by F-2Cl, while the absorption from 500 to 650 nm is mainly derived from the donors. These distinct absorption features allow us to quantify the compositions of constituent materials in the blends. Upon SVA treatment, all blend films presented red-shifted absorption due to the higher molecular ordering of both donor and acceptor molecules. Fig. 7c and d show that DRTT-T:F-2Cl and DRTT-R:F-2Cl films deposited from THF or CF and the CF-processed DRTT-OR:F-2Cl film all exhibited relatively homogeneous distribution of the donor and acceptor along the film-depth direction. This suggests that the interpenetrated donor and acceptor phases exist in the entire film-depth direction, providing interpenetrated pathways for holes and electrons. The overall higher content of the donor results from more donor components in the solution (donor : acceptor ratio = 1 : 0.75). Compared to DRTT-R:F-2Cl and DRTT-T:F-2Cl blend films with a donor content of *ca.* 55–65% and *ca.* 56–60% at the top part of the film, respectively, the DRTT-OR:F-2Cl blend showed a higher donor content of *ca.* 73–82%, which could be detrimental to electron collection by the top cathode. For the DRTT:F-2Cl blend film, a donor content of $\sim 100\%$ was observed in the film-depth range from 0 to ~ 40 nm, in combination of a significant enrichment of acceptor components (*ca.* 67–80%) at the bottom part of the film. Such a vertical gradient in the DRTT:F-2Cl blend film would obstruct charge collection and largely reduce the interface between the donor and the acceptor, thus resulting in the low J_{sat} in the OSC device. The donor and acceptor distribution along the film-depth direction is likely due to the solubility difference between the donor and acceptor materials. DRTT showed much lower solubility (8 mg mL^{-1}) than that of F-2Cl (90 mg mL^{-1}), so that DRTT molecules precipitated from the solution earlier than F-2Cl during the film-casting process leading to the extremely inhomogeneous vertical distribution. Similarly, solubility-mismatch-induced phase separation has been recently observed for poly(3-hexylthiophene):acceptor BHJ films.⁵⁹ By contrast, the

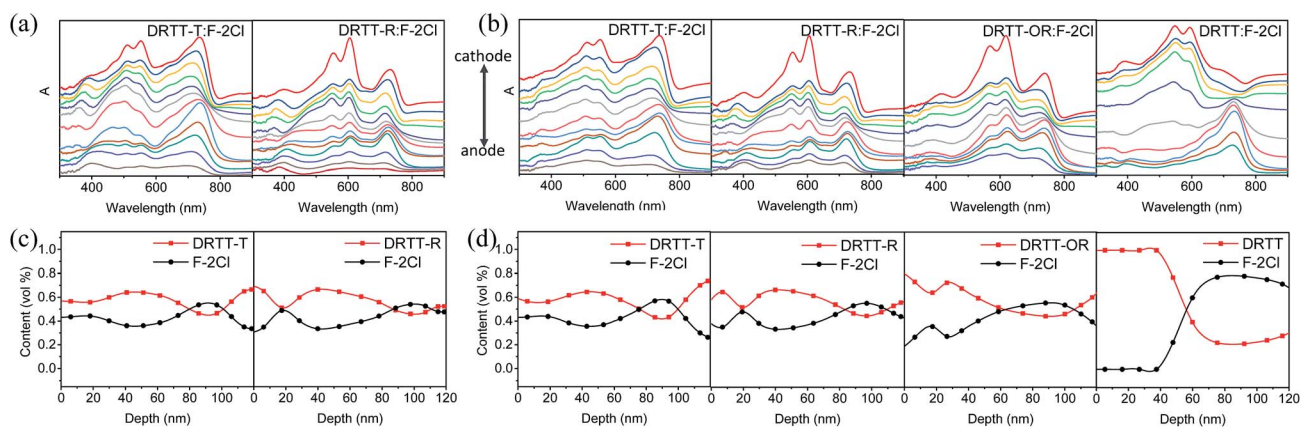


Fig. 7 Film-depth-dependent light absorption spectra of the blend films processed with THF (a) and CF (b) upon SVA treatments, and distribution of the donor and the acceptor in the blend films processed with THF (c) and CF (d) upon SVA treatments along the vertical direction as obtained from the real-time absorption spectra. In (a) and (b), for clarity the spectra have been vertically re-aligned, and each spectrum corresponds to a sub-layer with thickness *ca.* 10 nm. In (c) and (d), depths 0 nm and 120 nm represent PDINO/active layer and active layer/PEDOT:PSS interfaces, respectively.

solubilities of DRTT-T and DRTT-R in THF or CF were more close to that of F-2Cl, which contributed to uniform donor and acceptor distribution along the film-depth direction.

Conclusions

In summary, we have synthesized four wide-bandgap small molecule donors, *i.e.*, DRTT-T, DRTT-R, DRTT-OR and DRTT, to study the influence of conjugated backbone “twisting” on their properties. The molecules (DRTT-T and DRTT-R) with “twisted” backbones exhibited good solubility in the “green” solvent THF and a slow self-organization rate in the film-forming process. Ordered molecular packing with preferred face-on orientation and proper phase-separation morphology with homogeneous vertical distribution of donor and acceptor components were achieved in their BHJ films through prolonging the molecular self-organization time. As a result, high PCEs of 9.37% and 10.45% were achieved for DRTT-T and DRTT-R based NFSM-OSCs, respectively, when THF was used as the processing solvent. In contrast, the molecules (DRTT-OR and DRTT) with much more planar structures showed lower solubility in THF, and the devices could be fabricated with CF. However, the strong aggregation ability and low solubility of DRTT-OR and DRTT induced excessive phase separation and unfavorable vertical gradients of donor and acceptor components, thus leading to inferior device efficiencies. Our study demonstrates that appropriately “twisting” conjugated backbones can endow the conjugated molecules with much improved solubility in “green” solvents together with proper aggregation behavior and microstructure in films, providing an effective molecular design strategy for high-performance “green”-solvent-processed NFSM-OSCs.

Conflicts of interest

There are no conflicts to declare.

Acknowledgements

The authors acknowledge the National Natural Science Foundation of China (no. 21574128 and 51703158) and China Scholarship Council (no. 201806255059). L. Ye and H. Ade were supported by the U.S. Office of Naval Research Under Award No. N000141712204. This research used resources (SAXS/WAXS beamline 7.3.3) of the Advanced Light Source, which is a U.S. DOE Office of Science User Facility under contract no. DE-AC02-05CH11231. C. Zhu is appreciated for beamline support.

Notes and references

- G. Yu, J. Gao, J. C. Hummelen, F. Wudl and A. J. Heeger, *Science*, 1995, **270**, 1789.
- R. F. Service, *Science*, 2011, **332**, 293.
- G. Li, R. Zhu and Y. Yang, *Nat. Photonics*, 2012, **6**, 153.
- C.-C. Chueh, K. Yao, H.-L. Yip, C.-Y. Chang, Y.-X. Xu, K.-S. Chen, C.-Z. Li, P. Liu, F. Huang, Y. Chen, W.-C. Chen and A. K. Y. Jen, *Energy Environ. Sci.*, 2013, **6**, 3241.
- J. Zhao, Y. Li, G. Yang, K. Jiang, H. Lin, H. Ade, W. Ma and H. Yan, *Nat. Energy*, 2016, **1**, 15027.
- L. Ye, Y. Xiong, Q. Zhang, S. Li, C. Wang, Z. Jiang, J. Hou, W. You and H. Ade, *Adv. Mater.*, 2018, **30**, 1705485.
- W. Zhao, S. Zhang, Y. Zhang, S. Li, X. Liu, C. He, Z. Zheng and J. Hou, *Adv. Mater.*, 2018, **30**, 1704837.
- Z. Abbas, J. Shin, R. Atla, S. Rasool, C. E. Song, H. K. Lee, S. K. Lee, W. S. Shin, W. W. So, S. K. Kwon, Y. H. Kim and J. C. Lee, *ACS Appl. Mater. Interfaces*, 2018, **10**, 39107.
- C.-H. Zhang, W. Wang, W. Huang, J. Wang, Z. Hu, Z. Lin, T. Yang, F. Lin, Y. Xing, J. Bai, H. Sun and Y. Liang, *Chem. Mater.*, 2019, **31**, 3025.
- S. E. Shaheen, C. J. Brabec, N. S. Sariciftci, F. Padinger, T. Fromherz and J. C. Hummelen, *Appl. Phys. Lett.*, 2001, **78**, 841.
- K. Gao, S. B. Jo, X. Shi, L. Nian, M. Zhang, Y. Kan, F. Lin, B. Kan, B. Xu, Q. Rong, L. Shui, F. Liu, X. Peng, G. Zhou, Y. Cao and A. K. Jen, *Adv. Mater.*, 2019, **31**, 1807842.
- Y. Huo, H.-L. Zhang and X. Zhan, *ACS Energy Lett.*, 2019, **4**, 1241.
- L. Yang, S. Zhang, C. He, J. Zhang, H. Yao, Y. Yang, Y. Zhang, W. Zhao and J. Hou, *J. Am. Chem. Soc.*, 2017, **139**, 1958.
- H. Bin, Y. Yang, Z.-G. Zhang, L. Ye, M. Ghasemi, S. Chen, Y. Zhang, C. Zhang, C. Sun, L. Xue, C. Yang, H. Ade and Y. Li, *J. Am. Chem. Soc.*, 2017, **139**, 5085.
- X. Liu, Y. Sun, L. A. Perez, W. Wen, M. F. Toney, A. J. Heeger and G. C. Bazan, *J. Am. Chem. Soc.*, 2012, **134**, 20609.
- H. Li, Q. Wu, R. Zhou, Y. Shi, C. Yang, Y. Zhang, J. Zhang, W. Zou, D. Deng, K. Lu and Z. Wei, *Adv. Energy Mater.*, 2018, **9**, 1803175.
- Z. Zhou, S. Xu, J. Song, Y. Jin, Q. Yue, Y. Qian, F. Liu, F. Zhang and X. Zhu, *Nat. Energy*, 2018, **3**, 952.
- X. Liu, Y. Sun, B. B. Y. Hsu, A. Lorbach, L. Qi, A. J. Heeger and G. C. Bazan, *J. Am. Chem. Soc.*, 2014, **136**, 5697.
- Y. Lin, J. Wang, Z. G. Zhang, H. Bai, Y. Li, D. Zhu and X. Zhan, *Adv. Mater.*, 2015, **27**, 1170.
- Y. Lin, Q. He, F. Zhao, L. Huo, J. Mai, X. Lu, C. J. Su, T. Li, J. Wang, J. Zhu, Y. Sun, C. Wang and X. Zhan, *J. Am. Chem. Soc.*, 2016, **138**, 2973.
- P. Cheng, G. Li, X. Zhan and Y. Yang, *Nat. Photonics*, 2018, **12**, 131.
- D. Meng, D. Sun, C. Zhong, T. Liu, B. Fan, L. Huo, Y. Li, W. Jiang, H. Choi, T. Kim, J. Y. Kim, Y. Sun, Z. Wang and A. J. Heeger, *J. Am. Chem. Soc.*, 2016, **138**, 375.
- Z. P. Yu, Z. X. Liu, F. X. Chen, R. Qin, T. K. Lau, J. L. Yin, X. Kong, X. Lu, M. Shi, C. Z. Li and H. Chen, *Nat. Commun.*, 2019, **10**, 2152.
- J. Yuan, Y. Zhang, L. Zhou, G. Zhang, H.-L. Yip, T.-K. Lau, X. Lu, C. Zhu, H. Peng, P. A. Johnson, M. Leclerc, Y. Cao, J. Ulanski, Y. Li and Y. Zou, *Joule*, 2019, **3**, 1140.
- B. Kan, M. Li, Q. Zhang, F. Liu, X. Wan, Y. Wang, W. Ni, G. Long, X. Yang, H. Feng, Y. Zuo, M. Zhang, F. Huang, Y. Cao, T. P. Russell and Y. Chen, *J. Am. Chem. Soc.*, 2015, **137**, 3886.
- Y. Qin, L. Ye, S. Zhang, J. Zhu, B. Yang, H. Ade and J. Hou, *J. Mater. Chem. A*, 2018, **6**, 4324.

- 27 B. Fan, L. Ying, Z. Wang, B. He, X.-F. Jiang, F. Huang and Y. Cao, *Energy Environ. Sci.*, 2017, **10**, 1243.
- 28 Z. Li, L. Ying, P. Zhu, W. Zhong, N. Li, F. Liu, F. Huang and Y. Cao, *Energy Environ. Sci.*, 2019, **12**, 157.
- 29 Z. Zheng, O. M. Awartani, B. Gautam, D. Liu, Y. Qin, W. Li, A. Bataller, K. Gundogdu, H. Ade and J. Hou, *Adv. Mater.*, 2017, **29**, 1604241.
- 30 J. Wan, X. Xu, G. Zhang, Y. Li, K. Feng and Q. Peng, *Energy Environ. Sci.*, 2017, **10**, 1739.
- 31 L. Huo, S. Zhang, X. Guo, F. Xu, Y. Li and J. Hou, *Angew. Chem., Int. Ed.*, 2011, **50**, 9697.
- 32 R. Duan, L. Ye, X. Guo, Y. Huang, P. Wang, S. Zhang, J. Zhang, L. Huo and J. Hou, *Macromolecules*, 2012, **45**, 3032.
- 33 Y. Liu, C. e. Zhang, D. Hao, Z. Zhang, L. Wu, M. Li, S. Feng, X. Xu, F. Liu, X. Chen and Z. Bo, *Chem. Mater.*, 2018, **30**, 4307.
- 34 Y. Liu, Z. Zhang, S. Feng, M. Li, L. Wu, R. Hou, X. Xu, X. Chen and Z. Bo, *J. Am. Chem. Soc.*, 2017, **139**, 3356.
- 35 H. Yao, Y. Chen, Y. Qin, R. Yu, Y. Cui, B. Yang, S. Li, K. Zhang and J. Hou, *Adv. Mater.*, 2016, **28**, 8283.
- 36 O. Inganäs, W. R. Salaneck, J. E. Österholm and J. Laakso, *Synth. Met.*, 1988, **22**, 395.
- 37 Y. Liu, J. Zhao, Z. Li, C. Mu, W. Ma, H. Hu, K. Jiang, H. Lin, H. Ade and H. Yan, *Nat. Commun.*, 2014, **5**, 5293.
- 38 H. Hu, P. C. Y. Chow, G. Zhang, T. Ma, J. Liu, G. Yang and H. Yan, *Acc. Chem. Res.*, 2017, **50**, 2519.
- 39 M. Scheuble, Y. M. Gross, D. Trefz, M. Brinkmann, J. T. López Navarrete, M. C. Ruiz Delgado and S. Ludwigs, *Macromolecules*, 2015, **48**, 7049.
- 40 X. Dong, H. Tian, Z. Xie, Y. Geng and F. Wang, *Polym. Chem.*, 2017, **8**, 421.
- 41 M. He, M. Li, X. Dong, H. Tian, H. Tong, J. Liu, Z. Xie, Y. Geng and F. Wang, *J. Mater. Chem. A*, 2017, **5**, 20473.
- 42 Z.-G. Zhang, B. Qi, Z. Jin, D. Chi, Z. Qi, Y. Li and J. Wang, *Energy Environ. Sci.*, 2014, **7**, 1966.
- 43 Y. Wang, Y. Wang, B. Kan, X. Ke, X. Wan, C. Li and Y. Chen, *Adv. Energy Mater.*, 2018, **8**, 1802021.
- 44 M. Li, F. Liu, X. Wan, W. Ni, B. Kan, H. Feng, Q. Zhang, X. Yang, Y. Wang, Y. Zhang, Y. Shen, T. P. Russell and Y. Chen, *Adv. Mater.*, 2015, **27**, 6296.
- 45 M. D. Perez, C. Borek, S. R. Forrest and M. E. Thompson, *J. Am. Chem. Soc.*, 2009, **131**, 9281.
- 46 B. Xiao, M. Zhang, J. Yan, G. Luo, K. Gao, J. Liu, Q. You, H.-B. Wang, C. Gao, B. Zhao, X. Zhao, H. Wu and F. Liu, *Nano Energy*, 2017, **39**, 478.
- 47 X. Li, Y. Wang, Q. Zhu, X. Guo, W. Ma, X. Ou, M. Zhang and Y. Li, *J. Mater. Chem. A*, 2019, **7**, 3682.
- 48 L. Yang, S. Zhang, C. He, J. Zhang, Y. Yang, J. Zhu, Y. Cui, W. Zhao, H. Zhang, Y. Zhang, Z. Wei and J. Hou, *Chem. Mater.*, 2018, **30**, 2129.
- 49 B. Qiu, L. Xue, Y. Yang, H. Bin, Y. Zhang, C. Zhang, M. Xiao, K. Park, W. Morrison, Z.-G. Zhang and Y. Li, *Chem. Mater.*, 2017, **29**, 7543.
- 50 B. Kan, Q. Zhang, M. Li, X. Wan, W. Ni, G. Long, Y. Wang, X. Yang, H. Feng and Y. Chen, *J. Am. Chem. Soc.*, 2014, **136**, 15529.
- 51 Q. Wang, Y. Xie, F. Soltani-Kordshuli and M. Eslamian, *Renewable Sustainable Energy Rev.*, 2016, **56**, 347.
- 52 A. Maurano, R. Hamilton, C. G. Shuttle, A. M. Ballantyne, J. Nelson, B. O'Regan, W. Zhang, I. McCulloch, H. Azimi, M. Morana, C. J. Brabec and J. R. Durrant, *Adv. Mater.*, 2010, **22**, 4987.
- 53 A. Baumann, J. Lorrman, D. Rauh, C. Deibel and V. Dyakonov, *Adv. Mater.*, 2012, **24**, 4381.
- 54 A. Hexemer, W. Bras, J. Glossinger, E. Schaible, E. Gann, R. Kirian, A. MacDowell, M. Church, B. Rude and H. Padmore, *J. Phys.: Conf. Ser.*, 2010, **247**, 012007.
- 55 L. Bu, S. Gao, W. Wang, L. Zhou, S. Feng, X. Chen, D. Yu, S. Li and G. Lu, *Adv. Electron. Mater.*, 2016, **2**, 1600359.
- 56 S. Gao, L. Bu, Z. Zheng, X. Wang, W. Wang, L. Zhou, J. Hou and G. Lu, *AIP Adv.*, 2017, **7**, 045312.
- 57 Y. Huo, X.-T. Gong, T.-K. Lau, T. Xiao, C. Yan, X. Lu, G. Lu, X. Zhan and H.-L. Zhang, *Chem. Mater.*, 2018, **30**, 8661.
- 58 Y. Wang, Y. Zhang, G. Lu, X. Feng, T. Xiao, J. Xie, X. Liu, J. Ji, Z. Wei and L. Bu, *ACS Appl. Mater. Interfaces*, 2018, **10**, 13741.
- 59 Q. Liang, X. Jiao, Y. Yan, Z. Xie, G. Lu, J. Liu and Y. Han, *Adv. Funct. Mater.*, 2019, DOI: 10.1002/adfm.201807591.